Catalysis Today 288 (2017) 37–47

Contents lists available at ScienceDirect

Catalysis Today

journal homepage: www.elsevier.com/locate/cattod

Influence of the metal center of metalloprotoporphyrins on the electrocatalytic CO_2 reduction to formic acid

Yuvraj Y. Birdja[a], Jing Shen[a,b], Marc T.M. Koper[a,*]

[a] Leiden Institute of Chemistry, Leiden University, PO Box 9502, 2300 RA Leiden, The Netherlands
[b] Chemistry and Chemical Engineering Department, Hunan Institute of Engineering, Xiangtan, China

ARTICLE INFO

Article history:
Received 22 August 2016
Received in revised form 23 January 2017
Accepted 27 February 2017
Available online 23 March 2017

Keywords:
Carbon dioxide reduction
Hydrogen evolution
Formic acid formation
Immobilized molecular catalysts
Metalloporphyrins

ABSTRACT

Electrocatalytic conversion of carbon dioxide has gained much interest for the synthesis of value-added chemicals and solar fuels. Important issues such as high overpotentials and competition of hydrogen evolution still need to be overcome for deeper insight into the reaction mechanism in order to steer the selectivity towards specific products. Herein we report on several metalloprotoporphyrins immobilized on a pyrolytic graphite electrode for the selective reduction of carbon dioxide to formic acid. No formic acid is detected on Cr-, Mn-, Co- and Fe-protoporphyrins in perchloric acid of pH 3, while Ni-, Pd-, Cu- and Ga-protoporphyrins show only a little formic acid. Rh, In and Sn metal centers produce significant amounts of formic acid. However, the faradaic efficiency varies from 1% to 70% depending on the metal center, the pH of the electrolyte and the applied potential. The differentiation of the faradaic efficiency for formic acid on these metalloprotoporphyrins is strongly related to the activity of the porphyrin for the hydrogen evolution reaction. CO_2 reduction on Rh-protoporphyrin is shown to be coupled strongly to the hydrogen evolution reaction, whilst on Sn- and In-protoporphyrin such strong coupling between the two reactions is absent. The activity for the hydrogen evolution increases in the order In < Sn < Rh metal centers, leading to faradaic efficiency for formic acid increasing in the order Rh < Sn < In metal centers. In-protoporphyrin is the most stable and shows a high faradaic efficiency of ca. 70%, at a pH of 9.6 and a potential of −1.9 V vs RHE. Experiments in bicarbonate electrolyte were performed in an attempt to qualitatively study the role of bicarbonate in formic acid formation.

1. Introduction

In the past few decades the consequences of anthropogenic carbon dioxide accumulation in the atmosphere have been addressed repeatedly. It is nowadays generally accepted that the increasing carbon dioxide levels in the atmosphere pose serious problems if no action is taken [1]. The emission of CO_2 has increased since the industrial revolution, leading to an increased amount of CO_2 in the atmosphere [2]. Accumulation of atmospheric CO_2 leads to the greenhouse effect which contributes to global warming and climate change. Another important sustainability issue is the depletion of fossil fuel sources which is caused by an increasing world population and a changing lifestyle, resulting in an increasing energy demand. Mankind is still strongly dependent on fossil fuels for its energy consumption. A drawback of the use of fossil fuels is the production of CO_2 after combustion which is often simply released in the atmosphere. In the past couple of years much research has been done to mitigate CO_2 accumulation [3–6] and search for renewable energy sources [7–9]. A promising way to utilize CO_2 is by electrochemical CO_2 conversion. Compared to other methods the advantage of electrochemical conversion, when operational on an industrial scale, is two-fold: it reduces the CO_2 emissions in the atmosphere on one hand, and it produces renewable fuels and commodity chemicals on the other. Moreover, additional advantages are the fact that the process can be carried out at ambient conditions, water can be used as hydrogen source and, if the electricity used is produced from renewable sources, one can contribute to a completely sustainable carbon cycle. However, there are still significant hurdles which should be overcome or circumvented, such as the competition of the hydrogen evolution reaction, high overpotentials for CO_2 reduction, poor solubility of CO_2 in aqueous media and the poor selectivity for specific fuels. For implementation in the current infrastructure, liquid fuels are more convenient than gaseous fuels. Therefore much work has been focused on the

* Corresponding author.
E-mail address: m.koper@chem.leidenuniv.nl (M.T.M. Koper).

http://dx.doi.org/10.1016/j.cattod.2017.02.046

selective production of methanol, ethanol and formic acid. These fuels can be employed directly in fuel cells to produce electricity (e.g. Direct Methanol Fuel Cell and Direct Formic Acid Fuel Cell). Electroreduction of CO_2 to formic acid is less complex and therefore easier to optimize compared to alcohols, as only two electrons need to be transferred.

Molecular catalysts have been gaining more attention lately as they are relatively inexpensive and more abundantly available compared to (noble) metal catalysts. They usually show high activities and good selectivities for various reactions which can be tuned by modifying the catalyst with additional ligands, using electron-donating or electron-withdrawing groups [10–13]. In homogeneous electrocatalysis, these catalysts are often dissolved in non-aqueous solvents, as they are poorly soluble in aqueous electrolytes. Furthermore, large amounts of catalyst are needed to dissolve in the electrolyte. CO_2 can bind to a metal center which results in its activation [14] by a weakened C–O interaction due to transfer of electron density. After coordination to a metal center, reactions can take place which were initially not possible for free CO_2. Many different molecular catalysts have been reported for CO_2 reduction such as porphyrins, phthalocyanines, cyclams, phosphines and polypyridines [15,16].

Immobilization of molecular catalysts should in principle combine the best of both worlds: molecular catalysis on heterogeneous surfaces [17,18]. A system with high efficiency and selectivity can be created whereby the catalyst structure can be modified by addition of specific ligands e.g. to change the catalyst electronic properties which is very useful for mechanistic studies or controlling the selectivity. Furthermore, only a small amount of the catalyst is required and even catalysts insoluble in certain solvents can still be used when immobilized on a surface. Deactivation processes often encountered in homogeneous systems, such as dimerization and aggregation of the catalyst, can be circumvented. In the literature many different systems based on immobilized catalysts have been described: covalent attachment of the catalyst by using e.g. aryl diazonium salts, 4-aminopyridine [19–21], non-covalent attachment of the catalyst (drop-casting)[22,23] and dispersion of the catalyst in polymer films [24–27].

In this work we will focus on one type of molecular catalysts, namely metalloprotoporphyrins (MPPs) which are a subgroup of the more general metalloporphyrins. Metalloporphyrins are complexes that consist of a metal center within a heterocyclic macrocycle composed of four pyrrole groups attached to each other with methine bridges. Protoporphyrins have two vinyl, two propionic acid and four methyl groups attached to the porphyrin ring as shown in Fig. 1. Metalloprotoporphyrins are an important precursor for essential molecules in biology such as the heme-group in our red bloodcells and chlorophylls in plants (protoporphyrins with respectively an Fe^{2+} and Mg^{2+} metal centers). Furthermore it has been shown that (immobilized) metallo(proto)porphyrins are good catalysts for e.g. the oxygen reduction reaction, hydrogen evolution reaction, carbon dioxide reduction and nitrate reduction [28,10,16,29]. Savéant and Robert and coworkers have conducted extensive research on molecular catalysts for CO_2 reduction and how to influence the selectivity [30,31]. They recently showed that CO or HCOOH is produced by changing the metal center of the complex [32]. The selectivity issue is important from a fundamental point of view and therefore also the subject of theoretical studies [33,34], in which it has been shown that a different binding mode of CO_2 to the metal center leads to either CO or HCOOH.

In this paper, the selectivity towards formic acid is investigated experimentally where the role of the metal center is scrutinized by studying the pH effect, the concomitant hydrogen evolution and the nature of the electroactive species (i.e., CO_2 or HCO_3^-) on different metalloprotoporphyrins immobilized on pyrolytic graphite.

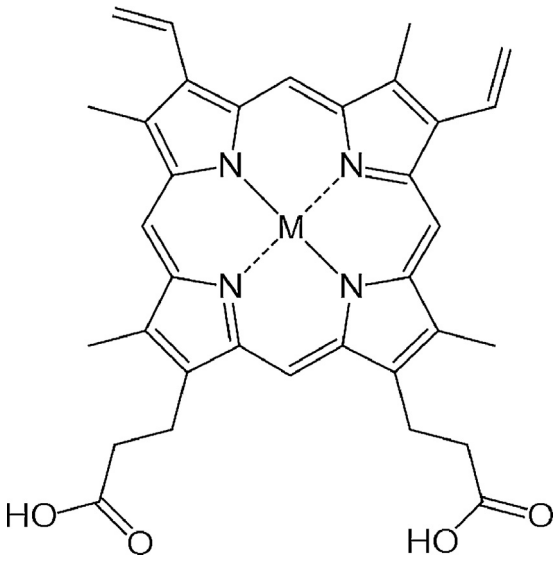

Fig. 1. Chemical structure metalloprotoporphyrins.

2. Experimental

The electrochemical experiments were performed in a one-compartment three-electrode cell at room temperature and ambient pressure. All glassware was first cleaned by boiling in a 1:1 mixture of concentrated sulfuric and nitric acid. Before each experiment the glassware was boiled three times in ultrapure water (Millipore MilliQ gradient A10 system, 18.2 MΩ cm). The long-term electrolysis experiments were carried out in a two-compartment three-electrode cell (H-type cell), where the working electrode (WE) and counter electrode (CE) compartments were separated by a nafion membrane (Nafion 115).

The WE was a pyrolytic graphite (PG) disc with a diameter of 5 mm or 10 mm used in a hanging meniscus configuration. The large PG electrodes were used for HPLC measurements to generate larger amounts of products. The reported current density is normalized by the geometric surface area of the WE. A platinum gauze and a reversible hydrogen electrode (RHE) in the same electrolyte were used as CE and reference electrode (RE), respectively. Unless mentioned otherwise, the potentials in this paper are referred to this reference electrode. Prior to each experiment, the WE was polished with sandpaper (first P600 and then P1000) and ultrasonicated for approximately 2–3 min in water. Blank cyclic voltammograms were recorded at a scan rate of 500 mV s^{-1} until a stable voltammogram was obtained (typically around 50 cycles) to ensure a clean PG surface. After immobilization of porphyrins a blank cyclic voltammogram was recorded again in order to qualitatively verify the immobilization of the porphyrin (as shown in Fig. S.1 in the SI). Metalloprotoporphyrins (MPPs) were immobilized on PG by drop casting from a 0.01 M borate solution of pH 10 in which the porphyrin was dissolved to a concentration of 0.5 mM [35].

Electrolyte solutions were prepared with ultrapure water. Pyrolytic graphite working electrodes were cut in-house from a high purity pyrolytic graphite plate (PY001009, Graphite Store, USA). High purity chemicals were used: perchloric acid and phosphoric acid (Merck Suprapur), potassium phosphate mono- and dibasic (Sigma Aldrich, TraceSelect), potassium phosphate tribasic (Sigma Aldrich, Reagent grade), sodium perchlorate (Sigma Aldrich, ACS reagent) and potassium bicarbonate (Sigma Aldrich, trace metals basis). All the porphyrins were purchased from Frontier Scientific and used without further purification. Before each experiment the cell was deaerated with argon (Linde, Argon 6.0 Scientific). For CO_2 reduction, the cell was saturated with CO_2 by

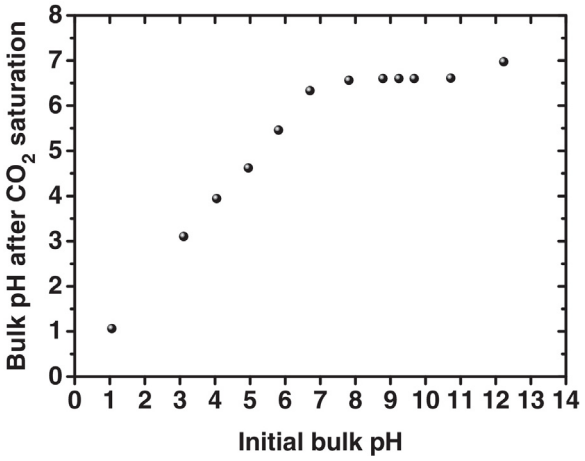

Fig. 2. Bulk pH of the used electrolytes before and after CO_2 saturation.

purging the cell with CO_2 (Linde, Carbon dioxide 4.5) for at least 20 min. Hydrogen 6.0 Scientific (Linde) was used for the RHE reference electrode. A μ-Autolab Type III (Metrohm Autolab B.V.) was used for voltammetric experiments with sample collection and an IviumStat or CompactStat (Ivium Technologies) was used to perform chronoamperometry and electrochemical impedance spectroscopy. Experiments were carried out in unbuffered perchloric acid of pH 1 and 3 and in a variety of different phosphate buffer solutions in the pH range of 3–12 (see Table S.1 in the Supporting Information). Although the actual pH will be lower when the electrolyte is saturated with CO_2, the different electrolytes will be referred to by their pH as measured prior to CO_2 saturation. Fig. 2 shows the relation between the pH before and after CO_2 saturation indicating that the pH after CO_2 saturation is approximately the same ($\approx$6.6) for almost all neutral and alkaline phosphate buffers. As we will see later, there are differences between these initially neutral and alkaline electrolytes in terms of faradaic efficiencies and product distribution. Therefore for a better discrimination between the different electrolytes we refer to them by the initial bulk pH. For correct measurements versus the RHE scale, the Luggin capillary and the RHE compartment were also filled with CO_2 saturated electrolyte. Furthermore, under reduction conditions, especially when H_2 is evolved, the pH near the electrode ("local pH") may differ from the pH in the bulk. This may affect the onset potential for product formation as well as product selectivity. As quite high currents were obtained, especially at the ø10 mm PG electrode, ohmic drop could not be neglected. Hence, the solution resistance was determined by potentiostatic electrochemical impedance spectroscopy. The obtained value was used to correct the voltammograms after the electrochemical data was collected. For chronoamperometry (electrolysis experiments) the potentiostat's IR compensation function was used to compensate for ohmic drop during measurement. Details can be found in the Supporting Information Section 2.

OnLine Electrochemical Mass Spectrometry (OLEMS) was utilized for the detection of volatile reaction products. A tip, which is placed close ($\approx$10 μm) to the electrode surface, continuously collects volatile reaction products from the electrode interface. The tip has a diameter of 0.5 mm and consists of a porous teflon cylinder (average pore size 10–14 μm) in a Kel-F holder and is connected to an EvoLution mass spectrometer (European Spectrometry Systems Ltd.) by a PEEK capillary [36]. A Quadrupole Mass Spectrometer Prisma QMS200 (Pfeiffer) is brought to vacuum with a TMH-071P turbo molecular pump (60 l s^{-1}, Pfeiffer) and a Duo 2.5 rotary vane pump (2.5 m^3 h^{-1}, Pfeiffer). Prior to experiments, the tip was cleaned in 0.2 M $K_2Cr_2O_7$ in 2 M H_2SO_4 and rinsed with ultrapure water. A SEM voltage between 1200 V and 2400 V was used for the different mass fragments. All mass fragments showed a decay during measurement which is the result of slow equilibration of the pressure in the system. This was corrected for by subtracting a double exponential fit to datapoints where no change in activity is observed from the whole dataset. The mass fragments shown in this paper are all background corrected in this manner.

Online High Performance Liquid Chromatography (online HPLC) is the technique employed to analyze non-volatile reaction products. A similar tip to the one for OLEMS, however, without a porous teflon cylinder, is placed near the electrode surface [37]. Samples with a volume of 60 μl were collected with a fraction collector (FRC-10A, Shimadzu) at a rate of 60 μl min^{-1} (LC-20AT pump, Shimadzu). Since the scan rate of the potential sweep during sample collection was 1 mV s^{-1}, each sample held the averaged concentration of a 60 mV potential difference. The samples were analyzed after voltammetry with HPLC (Prominence HPLC, Shimadzu). The samples were placed in an auto-sampler (SIL-20A) which injects 20 μl of the sample into the column. An Aminex HPX 87-H (Bio-Rad) column with a Micro-Guard Cation H Cartridge (Bio-Rad) in front were used. The eluent was 5 mM H_2SO_4 and the eluent flow rate 0.6 ml min^{-1}. The column and the refractive index detector (RID-10A) were maintained at a temperature of 35 °C.

The reported results were all reproduced at least twice and all electrochemical measurements (CV, OLEMS, online HPLC and Chronoamperometry) showed qualitatively the same results (HCOOH trend, current densities, onset potentials, etc.). From a quantitative point of view, the results sometimes could be slightly different, which is ascribed to a different PG surface each time after polishing the PG electrode as can be observed from the blank voltammograms recorded prior to the experiments. This is also the reason that for the standard error analysis in the HPLC results, only the concentration analysis of liquid phase is taken into account (concentrations are often low and the baseline noisy, which leads to different peak areas for different experiments).

3. Results and discussion

3.1. Activity of metalloprotoporphyrins in perchloric acid pH 3

For a proper attribution of the effect of the metal center on the activity or selectivity for the electrocatalytic CO_2 reduction, the influence of the bare substrate (PG) and the porphyrin macrocycle should first be known. Therefore, CO_2 reduction on pristine PG and on metal-less or free base PP immobilized on PG (denoted as PP-PG) was investigated. With online HPLC during voltammetry it was confirmed that no formic acid or other liquid products are produced at any potential on pristine PG nor on PP-PG. On-Line Electrochemical Mass Spectrometry showed that the only product from CO_2 reduction on PG and PP-PG is H_2 (see Fig. S.2 in the Supporting Information and also reference [38]).

Some of the investigated protoporphyrins with certain metal centers produce no formic acid or amounts lower than the detection limit. These protoporphyrins have a Cr, Mn, Co or Fe center. With OLEMS, no gaseous products other than H_2 are observed on MnPP, InPP, CrPP, SnPP and GaPP (Fig. S.4). On FePP, RhPP and CuPP small amounts of CH_4 are detected and on NiPP small amounts of CO and CH_4 are detected as shown in Fig. S.5. CoPP was recently shown to produce CO at pH 3 with high faradaic efficiency but no formic acid which is in agreement with our results. Moreover, a lower amount of CO was formed at pH 1 together with methane and a small amount of formic acid [38]. Comparing the curves in Fig. 3, it can be seen that PP-PG has a lower current compared to the pristine PG. The other MPPs show higher currents, indicating that the metalloprotoporphyrins are active for the hydrogen

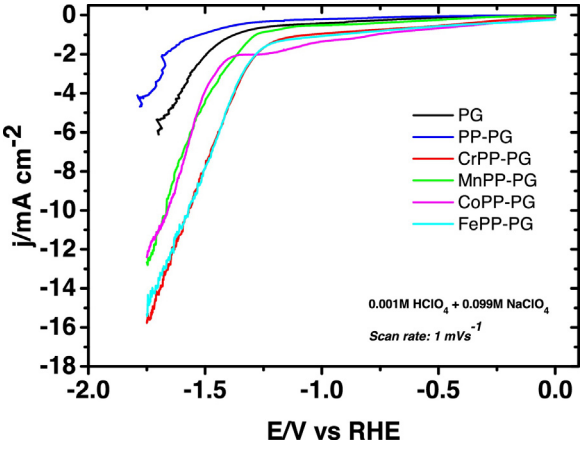

Fig. 3. Linear sweep voltammetry in CO_2 saturated 0.001 M $HClO_4$ + 0.099 M $NaClO_4$. Scan rate: 1 mV s^{-1}.

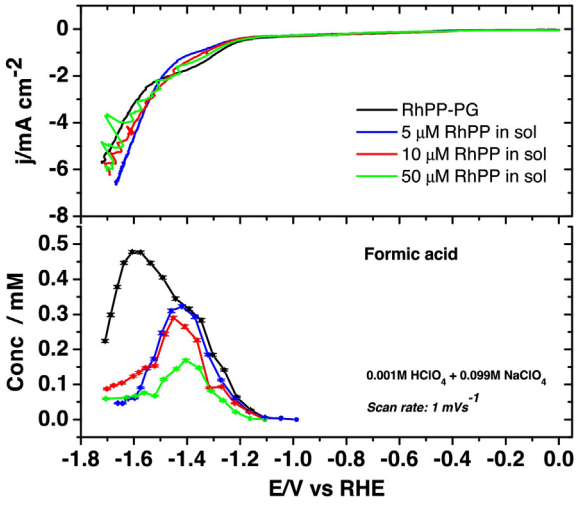

Fig. 5. CO_2 reduction on PG in RhPP containing electrolytes and immobilized RhPP on PG. Electrolyte solution 0.001 M $HClO_4$ + 0.099 M $NaClO_4$. Scan rate: 1 mV s^{-1}.

evolution reaction (HER) or CO_2 reduction, while PP presumably blocks active sites for HER and CO_2 reduction on PG. This confirms that the metal center is of importance for catalysis. The fluctuations in the CV at very negative potentials are the result of H_2 bubble formation and their detachment from the electrode surface. The current spikes appear skewed in some of the later voltammograms because of the post-measurement Ohmic drop correction.

In addition to the MPPs which are not active for formic acid production from CO_2, there is a set of MPPs which produce trace amounts of formic acid, as shown in Fig. 4a. These are the MPPs with Ni, Ga, Pd or Cu metal centers. The results have been reproduced and the standard errors in the concentration are shown in the graphs as well. OLEMS results again do not show significant amounts of other CO_2 reduction products besides H_2.

The most interesting MPPs for this study are SnPP, InPP and RhPP as these are able to produce significant amounts of formic acid from CO_2 as seen in Fig. 4b. As with the other MPPs there are no significant amounts of reaction products other than H_2 observed with OLEMS. All of these protoporphyrins show the same trend in formic acid concentration during Linear Sweep Voltammetry, with SnPP and RhPP having a slightly less negative onset potential for HCOOH formation than InPP. In and Sn metal centers were also identified to be active for CO_2 reduction to formic acid on phtalocyanines which are similar molecular catalysts to porphyrins [39]. More interesting is the fact that RhPP produces significant amounts of formic acid from CO_2. It has been reported that In and Sn metal electrodes mainly produce HCOOH, while Rh metal mostly forms H_2 [40]. Rh metal only shows activity for CO_2 reduction at elevated pressures [41]. Rh complexes have been shown to be active for hydrogenation of CO_2 to formic acid, albeit that they often do not operate in aqueous media without specific ligands [42–44]. Much research has been done on CO_2 hydrogenation to formic acid, but electrocatalytic reduction of CO_2 to formic acid on Rh porphyrins or similar Rh molecular catalysts has not been investigated in depth. Older work exists on Rh complexes dissolved in non-aqueous media [45,46] for which formic acid production was also observed.

In Fig. 5, a comparison is made between immobilized RhPP on PG and different amounts of RhPP in the electrolyte with a pristine PG electrode. The current densities and the trends in HCOOH concentration are similar. However, at a certain potential the formic acid concentration reaches a maximum and starts to decrease for RhPP in solution, while the RhPP-PG electrode continues to produce formic acid. The maximum for RhPP-PG is higher and at more negative potentials compared to RhPP in solution. Another observation is that a larger concentration of RhPP in solution leads to a lower amount of formic acid produced. This can be explained by inhibition of active sites with more RhPP molecules present in solution. These results show the superiority of immobilized

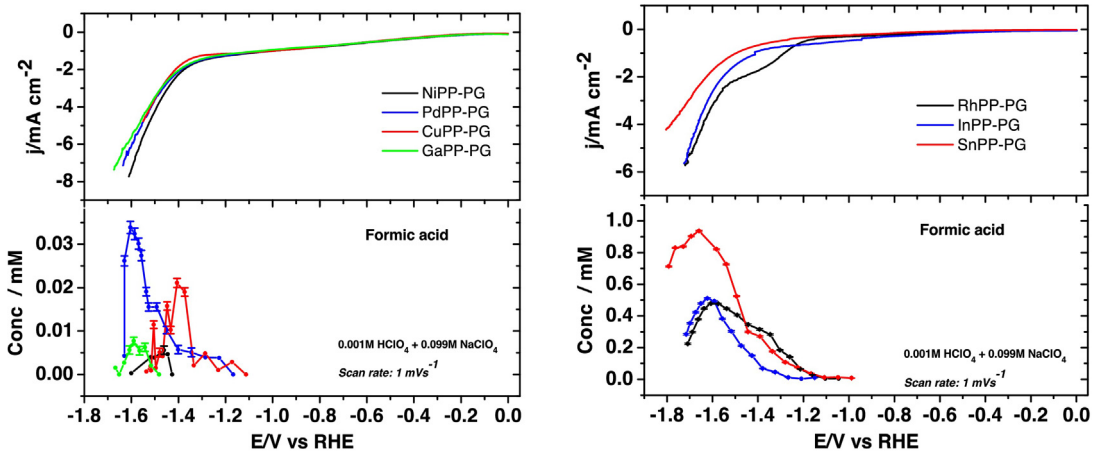

(a) Poorly active MPPs (b) Active MPPs

Fig. 4. Formic acid production on metalloprotoporphyrins in 0.001 M $HClO_4$ + 0.099 M $NaClO_4$. Scan rate: 1 mV s^{-1}.

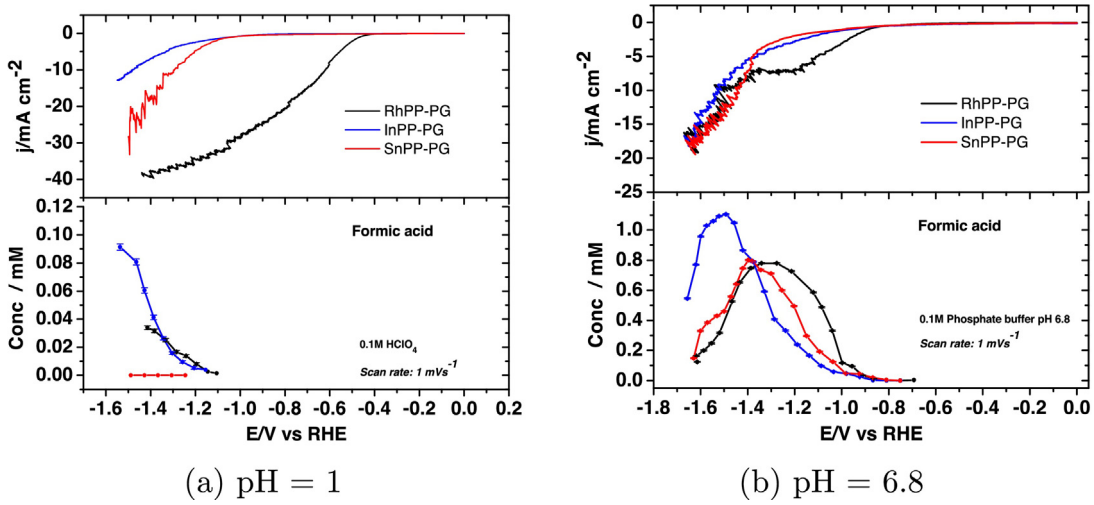

Fig. 6. CO_2 reduction on formic acid producing MPPs in (a) 0.1 M $HClO_4$ and (b) phosphate buffer of pH 6.8. Scan rate: 1 mV s^{-1}.

metalloprotoporphyrins with respect to metalloprotoporphyrins dissolved in the aqueous electrolyte.

3.2. Activity of metalloprotoporphyrins in other electrolytes

The formic acid producing MPPs from the previous paragraph were studied for their pH dependence is investigated in order to obtain more mechanistic insight. The aim is to deduce the origin of the activity of RhPP for CO_2 reduction to formic acid and identify possible differences between the MPPs as well as to identify the optimal conditions for formic acid formation.

In the 0.1 M $HClO_4$ electrolyte, all of these MPPs produce significantly less formic acid than in pH = 3 $HClO_4$ electrolyte as shown in Fig. 6a. Interestingly, a difference between the three formic acid producing MPPs is observed. In pH 1 InPP and RhPP still produce some HCOOH while SnPP only shows negligible amounts of HCOOH. The current generated by the InPP is much smaller compared to that of the other porphyrins. This is ascribed to a lower activity for hydrogen evolution, which also influences the faradaic efficiencies as will be discussed in a following section. Moreover, the onset potentials of the current profiles of the MPPs are quite different, in that RhPP has the least negative onset potential and InPP the most negative onset potential. This is probably associated with a difference in activity for the HER on these MPPs. In pH 6.8 (0.1 M phosphate buffer) comparable amounts of formic acid are formed as in pH 3, as illustrated in Fig. 6b.

Different phosphate buffer solutions were used for the study in electrolytes with a pH range from 3 till 12. Even though the bulk pH will be lower when the electrolyte is saturated with CO_2, the different electrolytes will be referred to by their pH as measured prior to CO_2 saturation. The formic acid production during the negative potential sweep on the three HCOOH-producing MPPs in the different electrolytes is shown in Figs. 7a–9a. The current profiles of RhPP show a plateau between −0.9 V and −1.5 V (see inset) while InPP and SnPP show no such plateau current (this is also visible in Figs. 4b and 6b). On RhPP the formic acid concentration profile shows a maximum which appears to be at potentials within this plateau region. Moreover, the HCOOH concentration profiles for RhPP are slightly shifted towards positive potentials for higher pH whereas those for InPP and SnPP do not show such a potential shift. This is better visible when the concentration profiles are normalized by their maximum concentration (as shown in Fig. S.6 in the SI). In the same Figs. 7b–9b the hydrogen evolution current on the three MPPs is shown in the same electrolytes. In these voltammograms no current plateau region is observed as for CO_2 reduction on RhPP, implying that this plateau feature is specifically related to CO_2 reduction. Moreover, there is a clear distinction between the current profiles in the different phosphate buffer electrolytes for all

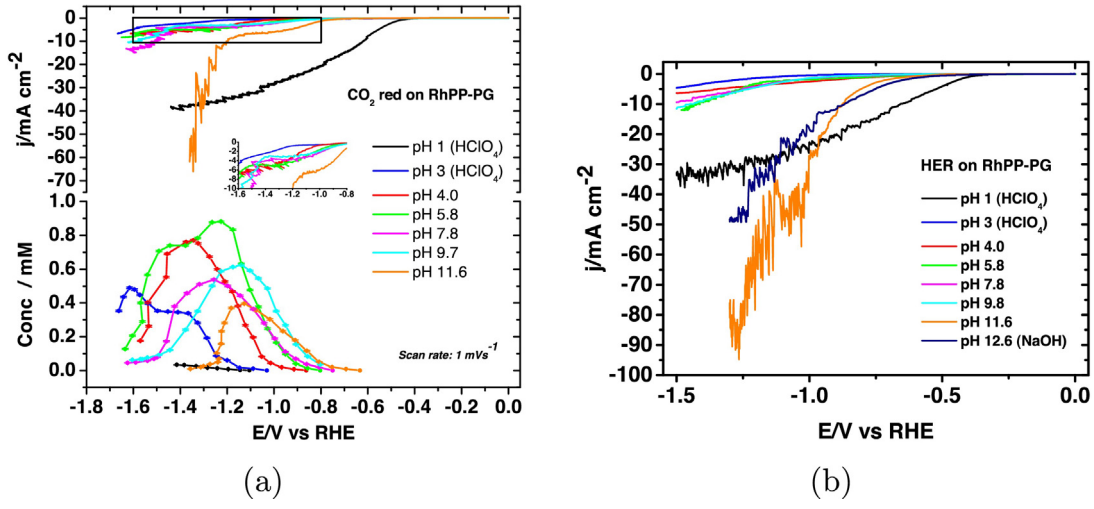

Fig. 7. CO_2 reduction (a) and hydrogen evolution (b) on RhPP in electrolytes with different pHs.

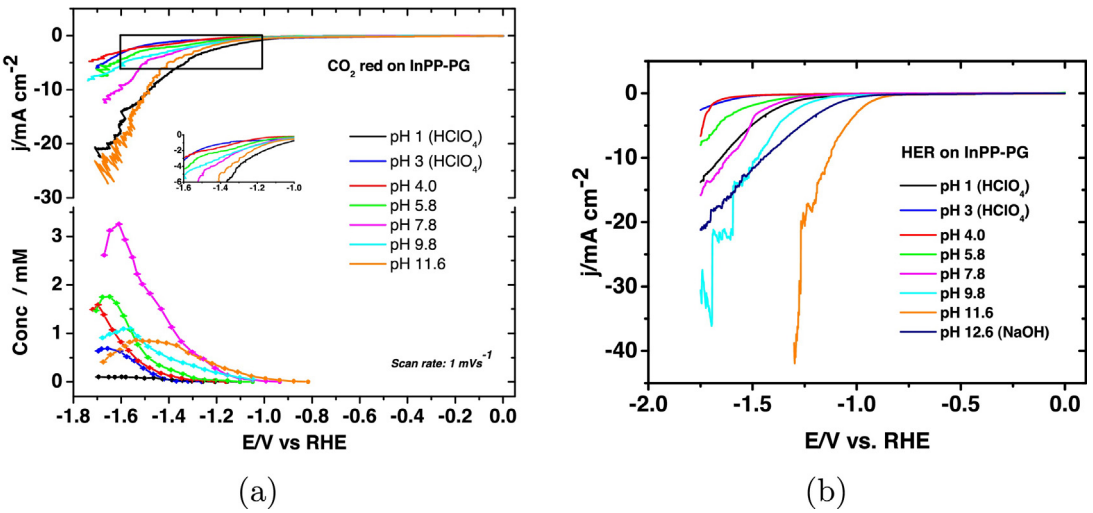

Fig. 8. CO_2 reduction (a) and hydrogen evolution (b) on InPP in electrolytes with different pHs.

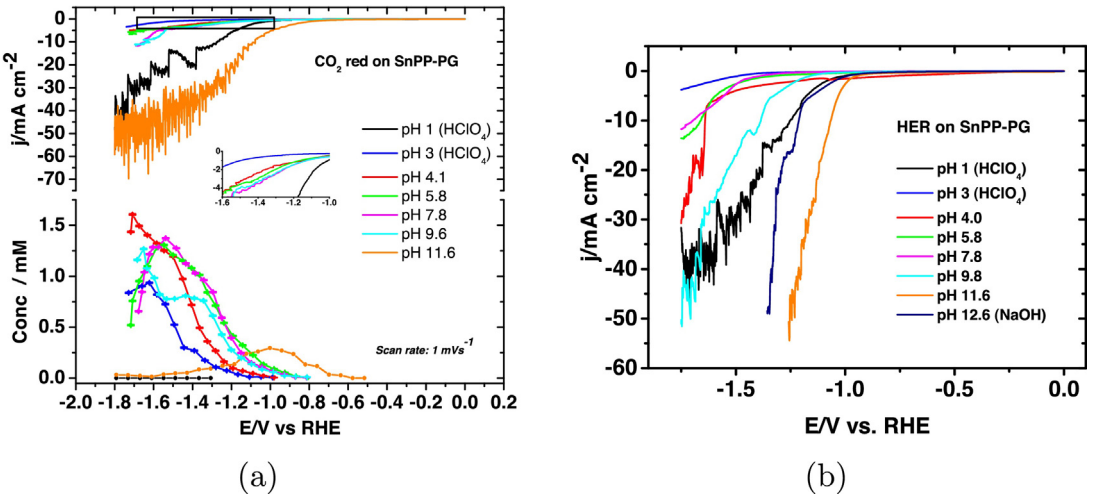

Fig. 9. CO_2 reduction (a) and hydrogen evolution (b) on SnPP in electrolytes with different pHs.

MPPs. The onset of hydrogen evolution seems strongly related to the pH of the phosphate buffers. At high pH (11.6) there is less negative onset of H_2 evolution and very high currents, while low pH (4 and 5.8) shows a more negative onset potential for HER and the currents are low. In general, the currents are much higher for RhPP compared to InPP and SnPP, indicating the better activity of RhPP for the HER. Comparing the current profiles for CO_2 reduction and HER on all three MPPs, the HER is somewhat inhibited by CO_2 reduction as the reduction onset is delayed to more negative potential and the currents are much lower. For RhPP the onset of the HER is close to/within the plateau region. The maximum HCOOH production also lies within this potential range and shifts to positive potentials with higher pH. As the maximum of HCOOH production can be interpreted to be the result of the competition between hydrogen evolution and CO_2 reduction, it seems plausible to associate the current plateau with this competition. The fact that the current plateau is not observed for InPP and SnPP could be due to the decoupling or weak coupling between CO_2 reduction and HER on these materials. The onset potential of the HER is more negative for SnPP and InPP compared to RhPP. The competition of CO_2 reduction and HER is important for high faradaic efficiencies towards HCOOH as will be discussed in a later section.

To investigate the pH effect more quantitatively, we define the onset potential for HCOOH and H_2. The onset potential is determined based on the HCOOH concentration profile and the current profiles. The onset potential based on the concentration is defined as the average potential of the potentials where the concentration of HCOOH reaches 0.01 mM, 0.03 mM and 0.05 mM. The potentials corresponding to these different concentrations lead to a similar trend. This is shown in Fig. S.7 in the Supporting Information. Similarly, the onset potential based on the current density is defined as the average of the potentials corresponding to different current densities within the range of 0.25–1 mA cm^{-2}. The onset potentials are converted to the NHE scale, and the trends for the 3 MPPs are shown in Fig. 10. The data within the shaded area correspond to the phosphate buffer electrolytes. Note that the analysis of the onset potentials is only performed for a better comparison between the different MPPs and not to derive underlying mechanistic information. The difference in pH before and after CO_2 saturation as mentioned in the experimental section, will not affect these results, since all the MPPs are measured in the same electrolyte. The buffer capacity of the electrolyte may play an important role on the selectivity for CO_2 reduction [47,48]. As shown in Fig. S.10, a higher buffer capacity leads to higher currents and affects the catalytic activity of the porphyrin towards formic acid. Therefore, the electrolyte pH is not the only factor influencing the catalytic activity of the immobilized porphyrins The onset potentials at pH 1 are quite different, because the influence of proton reduction

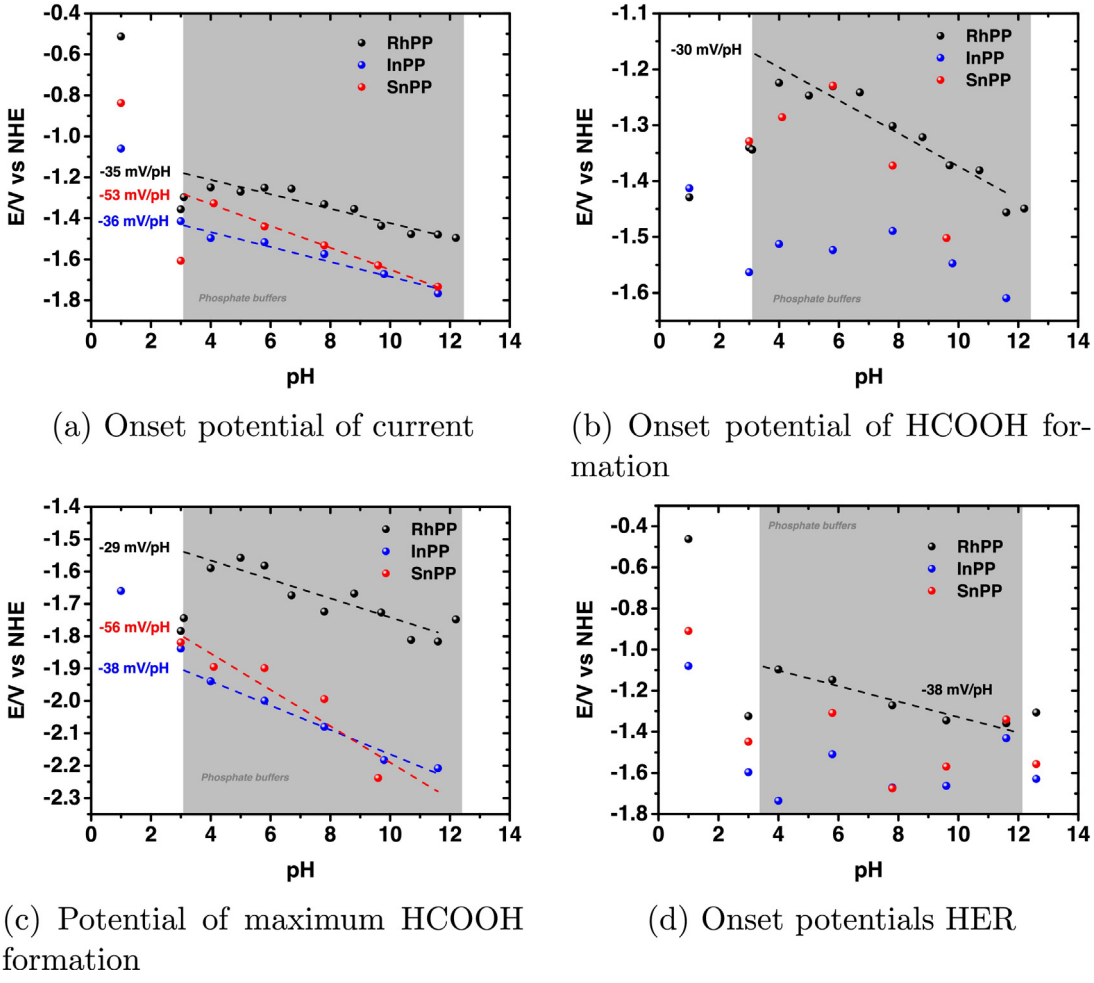

(a) Onset potential of current

(b) Onset potential of HCOOH formation

(c) Potential of maximum HCOOH formation

(d) Onset potentials HER

Fig. 10. Onset potentials based on (a) the current for CO_2-saturated solution, (b)the HCOOH concentration profile, (c) the maximum concentration of HCOOH and (d) the current of the HER.

is dominant here. As can be seen in Fig. 10a, the onset potential shows a linear dependence on pH for all MPPs. The pH dependence (slope) is not the same for the three MPPs. The onset potential of SnPP shifts with 53 ± 2 mV pH^{-1} while for InPP and RhPP they shift with 36 ± 5 and 35 ± 4 mV pH^{-1}. A slope of 59 mV pH^{-1} on the NHE potential scale would indicate a concerted proton–electron transfer mechanism [49]. It is difficult to say if SnPP follows a concerted proton–electron transfer mechanism solely based on the analysis of the onset potentials. However, the results indicate that there is probably a difference in mechanism between SnPP on one hand and RhPP and InPP on the other hand. Another distinction between SnPP and RhPP or InPP is the fact that at pH 11.6 only small amounts of HCOOH are formed on SnPP, while reasonable amounts of HCOOH are produced on InPP and RhPP. For RhPP similar pH dependences are observed for the onset of HCOOH and for H_2 formation (Fig. 10a and d), indicating that the CO_2 reduction to HCOOH on RhPP is coupled to the concomitant HER, as already suggested before. InPP and SnPP do not exhibit a clear linear pH dependence for HER (see Fig. 10d), which suggests that the trend observed in Fig. 10a is related to the CO_2 reduction rather than to the HER. On InPP and SnPP, CO_2 reduction and HER are not strongly coupled, as concluded before. On RhPP the potentials of maximum HCOOH production (Fig. 10c) show a similar slope to that of the onset potentials of HCOOH (Fig. 10b) confirming the earlier observation of a potential shift of the concentration profiles with pH, in contrast to InPP and SnPP where a similar slope is only observed for the HCOOH maxima and onset potential of the current (Figs. 10a and c). Furthermore, the onset potentials of RhPP are always at more positive potentials compared to those of InPP and SnPP. This difference in onset potentials confirms that RhPP is more active for the HER.

3.3. Faradaic efficiencies

For a further comparison of the activity between the MPPs, the faradaic efficiencies were determined during 2 h electrolysis in a two-compartment cell. The faradaic efficiencies for formic acid in $HClO_4$, pH 3 for all the three MPPs at different potentials are shown as function of time in Fig. 11. For RhPP and SnPP the faradaic efficiencies always decay with time to values of ≈1–2%. Interestingly InPP seems to reach a steady state value of ≈10–15%. This indicates that the immobilized porphyrins on PG are not very stable or deactivate rather quickly, especially RhPP-PG and SnPP-PG. Improving the performance of the immobilized porphyrins is beyond the scope of this paper. However, we believe that the deactivation is related to the catalyst instead of deposition of poisoning species on the surface or blockage of the active sites by intermediates. As shown in Fig. S.9 the blank voltammogram of the immobilized porphyrin on PG is compared with the blank voltammogram after CO_2 reduction or HER. It can be seen that the porphyrin-specific redox peaks have disappeared and the background current has changed. Therefore we believe that the decrease in activity is associated with

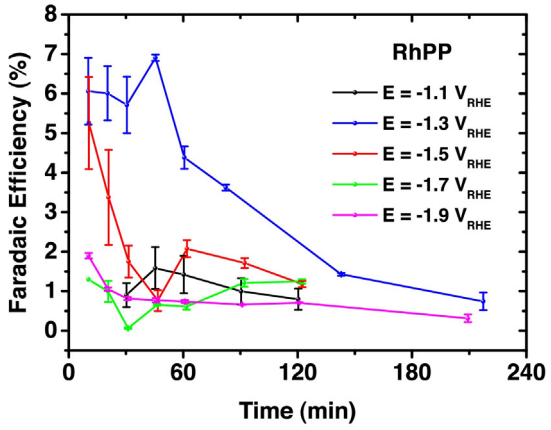

(a) RhPP

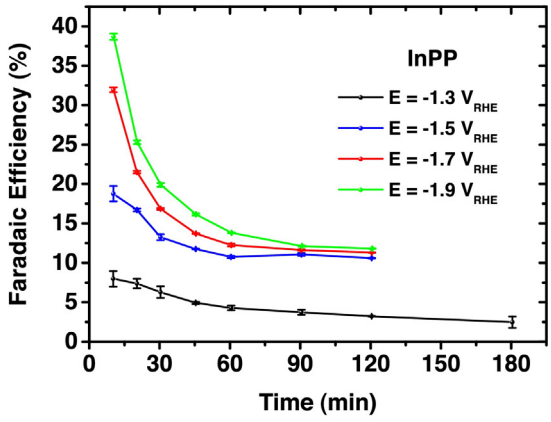

(b) InPP

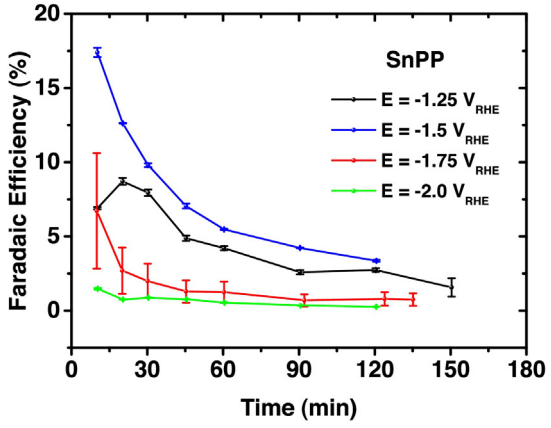

(c) SnPP

Fig. 11. Faradaic efficiencies in 0.001 M $HClO_4$ + 0.099 M $NaClO_4$ on different MPPs as function of time.

deactivation of the porphyrin structure or detachment of the porphyrin from PG. It is assumed that the very negative potentials ultimately are destructive for the immobilized porphyrins. RhPP shows lower faradaic efficiencies compared to SnPP which in turn is lower compared to InPP. The faradaic efficiencies determined after 10 min in $HClO_4$ pH = 3 are plotted against the applied potentials in Fig. 13a. The potential where the highest faradaic efficiencies are obtained in pH 3 is around $E = -1.3$ V for RhPP, around $E = -1.9$ V for InPP, and approximately $E = -1.5$ V for SnPP. This trend depends on the electrolyte, as can be seen in Fig. 12b, where the same is depicted for a phosphate buffer of pH 5.8. When only experiments at an applied potential of $E = -1.5$ V are considered, the influence of the pH can be revealed as seen in Fig. S.8 in the SI. The initial faradaic efficiency of the different MPPs as a function of pH is shown in Fig. 13. The faradaic efficiency of InPP at pH 9.6 seems to be optimal and reaches a value close to 70%.

3.4. Electroactive species

The fact that even in quite alkaline electrolytes HCOOH is produced, could indicate that not (only) CO_2 is the electroactive species but for instance bicarbonate is involved in the formation of formate. In the literature on electrocatalytic CO_2 reduction there has been controversy about the real electroactive species during CO_2 reduction at different pH and at different catalysts. Often dissolved CO_2 has been identified as the electroactive species [50,51], but there are also systems where bicarbonate has been suggested to be the key reactant specifically for the formation of formic acid/formate [52–56].

To probe the role of HCO_3^-, we studied different concentrations of $KHCO_3$ as electrolyte with and without CO_2 saturation. In Fig. 14a it is shown that a higher concentration of $KHCO_3$ leads to a larger amount of HCOOH formed on RhPP when no CO_2 is sparged through the solution. If the electrolyte is saturated with CO_2 an even larger amount of HCOOH is produced. This is observed for InPP and SnPP as well, as shown in Fig. 14b. The HCOOH concentration on InPP and SnPP is increased by a factor of more than 10 when CO_2 is purged through the solution. These results give a first impression that CO_2 should be the dominant electroactive species, however, it is still not conclusive enough to rule out HCO_3^- as reactive species. OLEMS experiments in $KHCO_3$ with and without CO_2 bubbling shown in Fig. 15, indicate that CO_2 does have an influence as the H_2 evolution and CO_2 consumption are delayed. Even without CO_2 saturation, the CO_2 mass signal decreases during the negative potential sweep implying that the origin of the formed HCOOH is the $KHCO_3$ electrolyte itself. However, during the negative potential sweep the pH in the vicinity of the working electrode increases as a result of the reactions shown in Eqs. (1) and (2). This higher local pH could lead to a local conversion of CO_2 to HCO_3^- (Eq. (3)), which may influence the direct bicarbonate reduction mechanism to formate. In previous studies, direct bicarbonate reduction has been suggested on palladium, lead and copper electrodes [53–56]. The experiments performed in this study only provide qualitative information about the influence of CO_2 and HCO_3^-. The simultaneous measurement of the local concentrations of formate, CO_2 and bicarbonate during voltammetry is crucial in order to shed more light on this debate.

$$2H^+ + 2e^- \rightarrow H_2 \quad (1)$$

$$2H_2O + 2e^- \rightarrow H_2 + 2OH^- \quad (2)$$

$$CO_2 + OH^- \rightarrow HCO_3^- \quad (3)$$

4. Conclusions

In this study we investigated the influence of the metal center of metalloprotoporphyrins for the electrocatalytic reduction of CO_2 towards formic acid. We found that Sn, In and Rh metal centers are able to produce significant amounts of HCOOH while Ni, Ga, Pd and Cu metal centers only show trace amounts of HCOOH. Metalloprotoporphyrins with Cr, Mn, Co or Fe centers do not produce measurable amounts of HCOOH. Moreover, immobilizing the MPPs on PG shows increased activity and stability compared to homogeneous catalysis with the complex in solution.

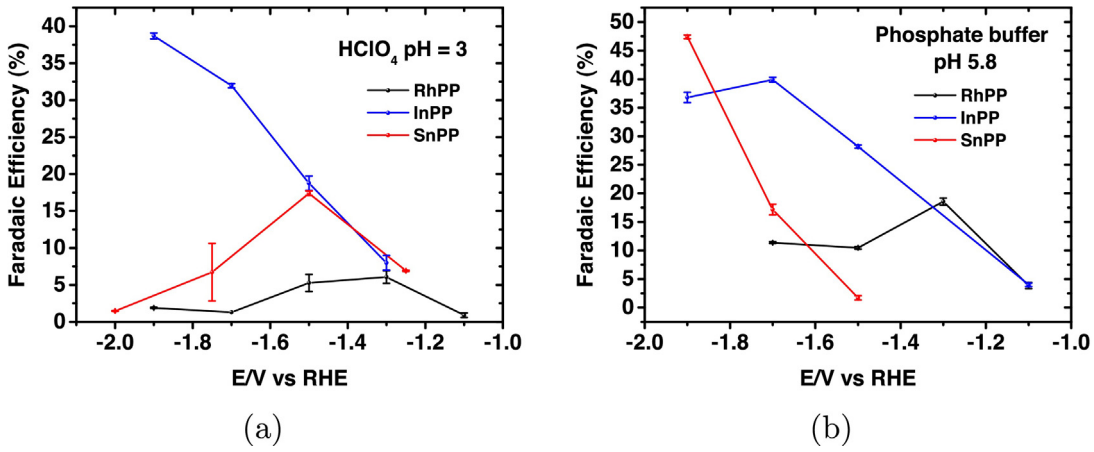

Fig. 12. Faradaic efficiencies determined at $t = 10$ min, as function of potential in (a) 0.001 M $HClO_4$ + 0.099 M $NaClO_4$ and (b) phosphate buffer of pH 5.8.

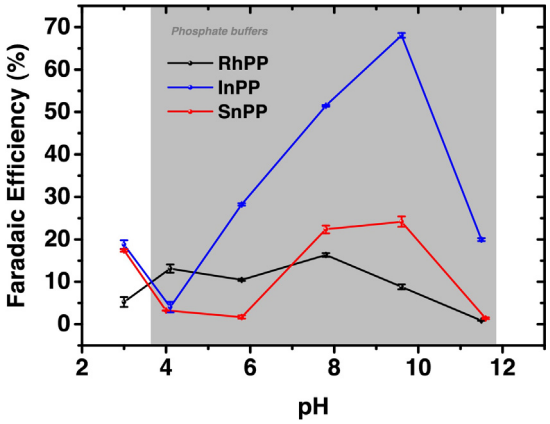

Fig. 13. Faradaic efficiencies determined at $t = 10$ min, at $E = -1.5$ V as function of pH.

The hydrogen evolution reaction plays an important role in the difference in activity towards HCOOH formation on RhPP, InPP and SnPP. RhPP is the most active for HER and InPP the least active. Consequently, InPP shows high faradaic efficiency towards HCOOH formation from CO_2 and RhPP low faradaic efficiency. SnPP lies in between with moderate activity for HER and faradaic efficiency towards HCOOH. All catalysts deactivate with time, however, the deactivation of InPP seems to be less compared to RhPP and SnPP.

All three HCOOH-producing MPPs show a pH dependence for CO_2 reduction as well as for HER. At very low pH, the proton reduction is dominant which results in little or no HCOOH formed. At very alkaline pHs, the HER also seems to be dominant, leading to poor selectivity towards HCOOH. The optimal pH is around 9.6 for InPP and between 7 and 10 for SnPP. The ideal situation (highest faradaic efficiencies) is different for the three MPPs in terms of electrolyte solution and applied potential. The best performance observed in this study is for InPP in pH 9.6 electrolyte where faradaic efficiencies of ≈70% were obtained.

This work highlights some important properties of metallo-protoporphyrins for electrocatalytic CO_2 reduction to formic acid. However, there is no consensus yet about the electroactive species for the formation of formic acid. Quantitative measurement of HCO_3^-, CO_2 and HCOOH concentrations during voltammetry would be necessary in this respect. For a detailed investigation of the mechanism, the support of theoretical calculations such as in Ref. [34] is also desirable.

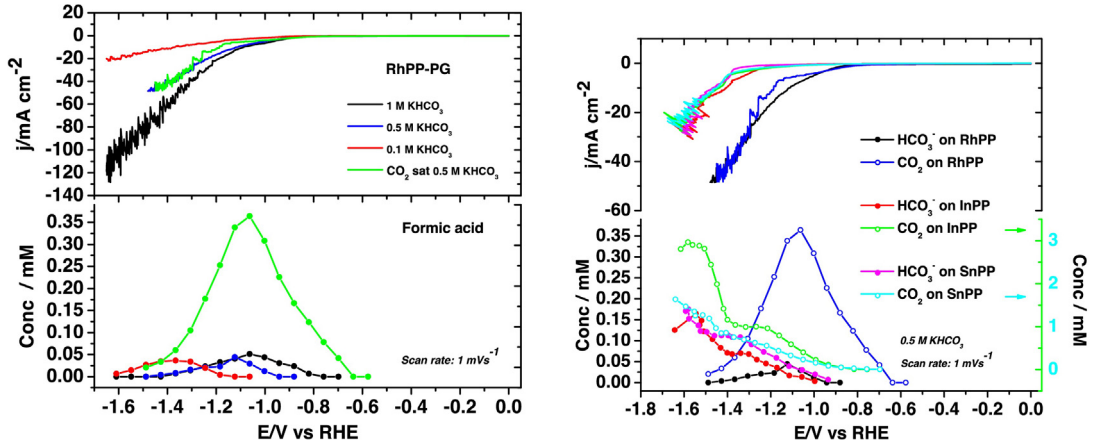

Fig. 14. CO_2/HCO_3^- reduction in $KHCO_3$ on the different MPPs. Scan rate: 1 mV s^{-1}.

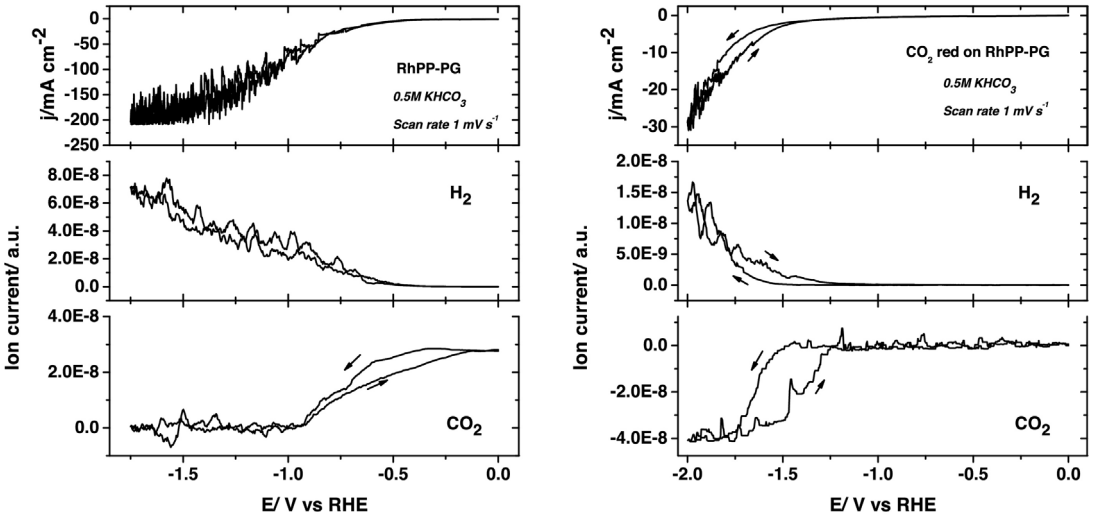

(a) Without CO_2 bubbling (b) With CO_2 bubbling

Fig. 15. H_2 and CO_2 signals during CO_2/HCO_3 reduction in 0.5 M $KHCO_3$. Scan rate: 1 mV s^{-1}.

Acknowledgement

J.S. acknowledges the award of a grant from the Chinese Scholarship Council.

Appendix A. Supplementary data

Supplementary data associated with this article can be found, in the online version, at http://dx.doi.org/10.1016/j.cattod.2017.02.046.

References

[1] I. Dincer, Environmental impacts of energy, Energy Policy 27 (1999) 845–854.
[2] R.K. Pachauri, L.A. Meyer (Eds.), Climate Change 2014: Synthesis Report. Contribution of Working Groups I, II and III to the Fifth Assessment Report of the Intergovernmental Panel on Climate Change, IPCC, Geneva, Switzerland, 2014.
[3] S. Bachu, CO_2 storage in geological media: role, means, status and barriers to deployment, Prog. Energy Combust. Sci. 34 (2008) 254–273.
[4] S.I. Plasynski, J.T. Litynski, H.G. McIlvried, R.D. Srivastava, Progress and new developments in carbon capture and storage, Crit. Rev. Plant Sci. 28 (2009) 123–138.
[5] M. Aresta, A. Dibenedetto, The contribution of the utilization option to reducing the CO_2 atmospheric loading: research needed to overcome existing barriers for a full exploitation of the potential of the CO_2 use, Catal. Today 98 (2004) 455–462.
[6] N.S. Spinner, J.A. Vega, W.E. Mustain, Recent progress in the electrochemical conversion and utilization of CO_2, Catal. Sci. Technol. 2 (2012) 19–28.
[7] N.L. Panwar, S.C. Kaushik, S. Kothari, Role of renewable energy sources in environmental protection: a review, Renew. Sustain. Energy Rev. 15 (2011) 1513–1524.
[8] H. Lund, Renewable energy strategies for sustainable development, Energy 32 (2007) 912–919.
[9] R. Baños, F. Manzano-Agugliaro, F.G. Montoya, A. Alcayde, C. Gil, J. Gómez, Optimization methods applied to renewable and sustainable energy: a review, Renew. Sustain. Energy Rev. 15 (2011) 1753–1766.
[10] A. Lü, Y. Fang, M. Zhu, S. Huang, Z. Ou, K.M. Kadish, Dioxygen reduction catalyzed by substituted iron tetraphenylporphyrins in acidic media, J. Porphyr. Phthalocyanines 16 (2012) 310–315.
[11] C. Costentin, S. Drouet, M. Robert, J.-M. Savant, A local proton source enhances CO_2 electroreduction to CO by a molecular Fe catalyst, Science 338 (6103) (2012) 90–94.
[12] S.-i. Yamazaki, Y. Yamada, S. Takeda, M. Goto, T. Ioroi, Z. Siromaa, K. Yasuda, Effects of p-substituents on electrochemical CO oxidation by Rh porphyrin-based catalysts, Phys. Chem. Chem. Phys. 12 (2010) 8968–8976.
[13] A. Ghosh, A comparison of ortho, meta, and para substituent effects in tetraphenylporphyrins: insights into the nature of the porphyrin-phenyl electronic interaction, J. Mol. Struct. (Theochem) 388 (1996) 359–363.
[14] M.E. Vol'pin, I.S. Kolomnikov, Reactions of carbon dioxide with transition metal compounds, Pure Appl. Chem. 33 (4) (1973) 567–582.
[15] E.E. Benson, C.P. Kubiak, A.J. Sathrum, J.M. Smieja, Electrocatalytic and homogeneous approaches to conversion of CO_2 to liquid fuels, Chem. Soc. Rev. 38 (2009) 89–99.
[16] J.L. Inglis, B.J. MacLean, M.T. Pryce, J.G. Vos, Electrocatalytic pathways towards sustainable fuel production from water and CO_2, Coord. Chem. Rev. 256 (2012) 2571–2600.
[17] R.W. Murray, Chemically modified electrodes, Acc. Chem. Res. 13 (1980) 135–141.
[18] W.A. Herrmann, C.W. Kohlpaintner, Water-soluble ligands, metal complexes, and catalysts: synergism of homogeneous and heterogeneous catalysis, Angew. Chem. Int. Ed. Engl. 32 (1993) 1524–1544.
[19] A. Yeşildağ, D. Ekinci, Covalent attachment of pyridine-type molecules to glassy carbon surfaces by electrochemical reduction of in situ generated diazonium salts. Formation of ruthenium complexes on ligand-modified surfaces, Electrochim. Acta 55 (2010) 7000–7009.
[20] T. Atoguchi, A. Aramata, A. Kazusaka, M. Enyo, Cobalt(II)-tetraphenylporphyrin-pyridine complex fixed on a glassy carbon electrode and its prominent catalytic activity for reduction of carbon dioxide, J. Chem. Soc., Chem. Commun. (1991) 156–157.
[21] T. Atoguchi, A. Aramata, A. Kazusaka, M. Enyo, Electrocatalytic activity of Coll TPP-pyridine complex modified carbon electrode for CO_2 reduction, J. Electroanal. Chem. 318 (1991) 309–320.
[22] T. Yoshida, K. Kamato, M. Tsukamoto, T. Iida, D. Schlettwein, M. Kaneko, D. Wohrle, Selective electrocatalysis for CO_2 reduction in the aqueous phase using cobalt phthalocyanine/poly-4-vinylpyridine modified electrodes, J. Electroanal. Chem. 385 (1995) 209–225.
[23] T. de Groot, Electrochemistry of Immobilized Hemes and Heme Proteins (PhD thesis), Eindhoven University of Technology, 2007.
[24] A. Deronzier, J.-C. Moute, Functionalized polypyrroles. New molecular materials for electrocatalysis and related applications, Acc. Chem. Res. 22 (1989) 249–255.
[25] J. Roncali, Electrogenerated functional conjugated polymers as advanced electrode materials, J. Mater. Chem. 9 (1999) 1875–1893.
[26] A. Bettelheim, B.A. White, S.A. Raybuck, R.W. Murray, Electrochemical polymerization of amino-, pyrrole-, and hydroxy-substituted tetraphenylporphyrin, Inorg. Chem. 26 (1987) 1009–1017.
[27] A. Giraudeau, D. Schaming, J. Hao, R. Farha, M. Goldmann, L. Ruhlmann, A simple way for the electropolymerization of porphyrins, J. Electroanal. Chem. 638 (2010) 70–75.
[28] R. Boulatov, Metalloporphyrin catalysts for oxygen reduction, in: M.T.M. Koper (Ed.), Fuel Cell Catalysis. A Surface Science Approach, John Wiley & Sons, Inc., New York, 2009, pp. 637–693, Chapter 18.
[29] J. Shen, Y.Y. Birdja, M.T.M. Koper, Electrocatalytic nitrate reduction by a cobalt protoporphyrin immobilized on a pyrolytic graphite electrode, Langmuir 31 (30) (2015) 8495–8501.
[30] C. Costentin, M. Robert, J.-M. Savant, Current issues in molecular catalysis illustrated by iron porphyrins as catalysts of the CO_2-to-CO electrochemical conversion, Acc. Chem. Res. 48 (2015) 2996–3006.
[31] A. Maurin, M. Robert, Noncovalent immobilization of a molecular iron-based electrocatalyst on carbon electrodes for selective, efficient CO_2-to-CO conversion in water, J. Am. Chem. Soc. 138 (2016) 2492–2495.

[32] L. Chen, Z. Guo, X.-G. Wei, C. Gallenkamp, J. Bonin, E. Anxolabhre-Mallart, K.-C. Lau, T.-C. Lau, M. Robert, Molecular catalysis of the electrochemical and photochemical reduction of CO_2 with earth-abundant metal complexes. Selective production of CO vs HCOOH by switching of the metal center, J. Am. Chem. Soc. 137 (34) (2015) 10918–10921.
[33] J. Shen, M.J. Kolb, A.J. Göttle, M.T.M. Koper, DFT study on the mechanism of the electrochemical reduction of CO_2 catalyzed by cobalt porphyrins, J. Phys. Chem. C 120 (29) (2016) 15714–15721.
[34] J.S. Yoo, R. Christensen, T. Vegge, J.K. Norskov, F. Studt, Theoretical insight into the trends that guide the electrochemical reduction of carbon dioxide to formic acid, ChemSusChem 9 (4) (2016) 358–363.
[35] M.T. de Groot, M.T.M. Koper, Redox transitions of chromium, manganese, iron, cobalt and nickel protoporphyrins in aqueous solution, Phys. Chem. Chem. Phys. 10 (2008) 1023–1031.
[36] A.H. Wonders, T.H.M. Housmans, V. Rosca, M.T.M. Koper, On-line mass spectrometry system for measurements at single-crystal electrodes in hanging meniscus configuration, J. Appl. Electrochem. 36 (2006) 1215–1221.
[37] Y. Kwon, M.T.M. Koper, Combining voltammetry with HPLC: application to electro-oxidation of glycerol, Anal. Chem. 82 (2010) 5420–5424.
[38] J. Shen, R. Kortlever, R. Kas, Y.Y. Birdja, O. Diaz-Morales, Y. Kwon, I. Ledezma-Yanez, K.J.P. Schouten, G. Mul, M.T.M. Koper, Electrocatalytic reduction of carbon dioxide to carbon monoxide and methane at an immobilized cobalt protoporphyrin, Nat. Commun. 6 (2015) 8177.
[39] N. Furuya, K. Matsui, Electroreduction of carbon dioxide on gas-diffusion electrodes modified by metal phthalocyanines, J. Electroanal. Chem. 271 (1989) 181–191.
[40] M. Azuma, K. Hashimoto, M. Hiramoto, M. Watanabe, T. Sakata, Electrochemical reduction of carbon dioxide on various metal electrodes in low-temperature aqueous $KHCO_3$ media, J. Electrochem. Soc. 137 (6) (1990) 1772–1778.
[41] Y. Hori, Modern Aspects of Electrochemistry, vol. 42, Springer, New York, 2008.
[42] F. Gassner, W. Leitner, Hydrogenation of carbon dioxide to formic acid using water-soluble rhodium catalysts, J. Chem. Soc., Chem. Commun. 19 (1993) 1465.
[43] J.-C. Tsai, K.M. Nicholas, Rhodium-catalyzed hydrogenation of carbon dioxide to formic acid, J. Am. Chem. Soc. 114 (1992) 5117–5124.
[44] F. Hutschka, A. Dedieu, M. Eichberger, R. Fornika, W. Leitner, Mechanistic aspects of the rhodium-catalyzed hydrogenation of CO_2 to formic acids – a theoretical and kinetic study, J. Am. Chem. Soc. 119 (1997) 4432–4443.
[45] S. Slater, J.H. Wagenknecht, Electrochemical reduction of CO_2 catalyzed by $Rh(diphos)_2Cl$, J. Am. Chem. Soc. 106 (1984) 5368–5370.
[46] C.M. Bolinger, N. Story, B.P. Sullivan, T.J. Meyer, Electrocatalytic reduction of carbon dioxide by 2,2′-bipyridine complexes of rhodium and iridium, Inorg. Chem. 27 (1988) 4582–4587.
[47] R. Kas, R. Kortlever, H. Yilmaz, M.T.M. Koper, G. Mul, Manipulating the hydrocarbon selectivity of copper nanoparticles in CO_2 electroreduction by process conditions, ChemElectroChem 2 (3) (2015) 354–358.
[48] A.S. Varela, M. Kroschel, T. Reier, P. Strasser, Controlling the selectivity of CO_2 electroreduction on copper: the effect of the electrolyte concentration and the importance of local pH, Catal. Today 260 (2016) 8–13.
[49] M.T.M. Koper, Theory of multiple proton–electron transfer reactions and its implications for electrocatalysis, Chem. Sci. 4 (2013) 2710–2723.
[50] P. van Rysselberghe, G.J. Alkire, J.M. McGee, Polarographic reduction of carbon dioxide. III. Description and interpretation of the waves, J. Am. Chem. Soc. 68 (1946) 2050–2055.
[51] T.E. Teeter, P. Van Rysselberghe, Reduction of carbon dioxide on mercury cathodes, J. Chem. Phys. 22 (1954) 759–760.
[52] M. Spichiger-Ulmann, J. Augustynski, Remarkable enhancement of the rate of cathodic reduction of hydrocarbonate anions at palladium in the presence of caesium cations, Helv. Chim. Acta 69 (1986) 632–634.
[53] M. Spichiger-Ulmann, J. Augustynski, Electrochemical reduction of bicarbonate ions at a bright palladium cathode, J. Chem. Soc. Faraday Trans. 81 (1985) 713–716.
[54] E.A. Kolyadko, B.I. Podlovchenko, S. Lu, Reduction of carbon dioxide on mercury cathodes, J. Electroanal. Chem. 373 (1994) 185–187.
[55] B. Innocent, D. Pasquier, F. Ropital, F. Hahn, J.-M. Leger, K.B. Kokoh, FTIR spectroscopy study of the reduction of carbon dioxide on lead electrode in aqueous medium, Appl. Catal. B: Environ. 94 (2010) 219–224.
[56] R. Kortlever, K.H. Tan, Y. Kwon, M.T.M. Koper, Electrochemical carbon dioxide and bicarbonate reduction on copper in weakly alkaline media, J. Solid State Electrochem. 17 (2013) 1843–1849.